



Immobilization of bioactive vascular endothelial growth factor onto Ca-deficient hydroxyapatite-coated Mg by covalent bonding using polydopamine

Junlei Li^{a,1}, Fang Cao^{b,1}, Bin Wu^a, Jiahui Yang^a, Wenwu Xu^a, Weidan Wang^a, Xiaowei Wei^a, Ge Liu^a, Dewei Zhao^{a,*}

^a Department of Orthopaedics, Affiliated Zhongshan Hospital of Dalian University, Dalian, 116001, China

^b Department of Biomedical Engineering, Faculty of Electronic Information and Electrical Engineering, Dalian University of Technology, Dalian, 116024, China

ARTICLE INFO

Keywords:

Magnesium
Bone tissue engineering
Angiogenesis
VEGF

ABSTRACT

Background: Bone tissue engineering (BTE) is considered a promising technology for repairing bone defects. Mg²⁺ promotes osteogenesis, which makes Mg-based scaffolds popular for research on orthopedic implant materials. Angiogenesis plays an important role in the process of bone tissue repair and regeneration, and it is one of the important problems in BTE urgently needs to be solved.

Methods: Mg was firstly coated with Ca-deficient hydroxyapatite (CDHA) via hydrothermal treatment, and polydopamine (DOPA) was then used as the connecting medium to immobilize vascular endothelial growth factor (VEGF) on the CDHA coating. The physicochemical properties of the coatings were characterized by SEM, EDS, XPS, FTIR and immersion experiment in SBF. The adhesion, proliferation, and angiogenesis potential of the coatings were determined in vitro.

Results: The composite coating significantly improved the corrosion resistance of Mg and prohibited excessively high local alkalinity. VEGF could be firmly immobilized on Mg via polydopamine. The CCK-8, live/dead staining and adhesion test results showed that the VEGF-DOPA-CDHA coating exhibited excellent biocompatibility and could significantly improve the adhesion and proliferation of MC3T3-E1 cells on Mg. Microtubule formation, immunofluorescence and Quantitative Real-Time PCR (qRT-PCR) experiments showed that VEGF immobilized on Mg still possessed bioactivity in promoting the differentiation of rat mesenchymal stem cells into endothelial cells.

Conclusion: In this study, we enabled the angiogenic biological activity of Mg by immobilizing VEGF on Mg. Mg was successfully coated with a functional VEGF-DOPA-CDHA composite coating. The CDHA coating significantly increased the corrosion resistance of Mg and prohibited the negative effect of excessively high local alkalinity on the biological activity of VEGF. As an intermediate layer, the DOPA coating protects Mg, and DOPA provides a binding site for VEGF so that VEGF can be firmly immobilized on Mg and give Mg angiogenic bioactivity during the initial period of implantation.

The translational potential of this article: The treatment of large bone defect is still one of the orthopedic trauma diseases that are difficult to be completely treated in clinic. The development of tissue engineering technology provides a new option for the treatment of large bone defects. The regeneration of blood vessels is of great significance for the repair of bone defects. In this study, VEGF was connected on the surface of degradable magnesium by covalent bonding. Vascular biofunctionalized magnesium scaffolds are expected to regenerate bone tissue with blood transport and be used in the clinical treatment of large bone defects.

1. Introduction

The therapy for bone defects caused by injury, infection, tumor

excision and congenital diseases is one of the commonest and most thorny problems in orthopedic clinics [1]. Bone defects smaller than the critical size can heal spontaneously, while large bone defects are usually

* Corresponding author.

E-mail address: zhaodewei2016@163.com (D. Zhao).

¹ Li Junlei and Cao Fang have made the same contribution to the article, and they are the co-first authors

<https://doi.org/10.1016/j.jot.2021.06.002>

Received 29 December 2020; Received in revised form 27 May 2021; Accepted 14 June 2021

difficult to repair spontaneously and need to be treated by bone transplantation or replacement implantation [2]. Autologous bone has the advantages of being osteoconductive, osteoinductive and angiogenic, and immune rejection is not problematic. These characteristics make autogenous bone the gold standard for bone defect treatment, but their limited availability is the main obstacle for the extensive application of autologous bone transplantation in clinical practice. In contrast, allogeneic bone transplantation does not have the advantages of being osteoconductive, osteoinductive and angiogenic and is also prone to cross infection, immune rejection and other problems [3]. Artificial scaffolds are considered a promising treatment for bone repair. The design of a biodegradable scaffold with excellent biocompatibility and mechanical properties, as well as a good ability to promote osteogenesis and vascularization, is of great significance for the repair and regeneration of bone defects [4].

Ceramic, polymer and metals have been widely studied as scaffolds for the repair and regeneration of bone defects [5]. Excellent mechanical properties are an important advantage of the use of metallic biomaterials as scaffold materials [6]. Porous titanium and tantalum can form an osseous bond with bone tissue [7]. Therefore, there have been many reports on the application of porous titanium and tantalum in bone defect repair and regeneration [8–11]. Both Ti- and Ta-based biomaterials are bioinert and have good stability in the human environment, which ensures good biocompatibility [12,13]. However, these two materials lack bioactivity to promote bone regeneration [14]. Among all medical metallic biomaterials, Mg, a biodegradable orthopedic implant biomaterial, has received extensive attention [15]. Mg exhibits excellent biocompatibility, and its mechanical properties are similar to those of cortical bone. Moreover, Mg^{2+} released by the degradation of Mg also has the advantage of being osteogenic [16–18]. Therefore, as an orthopedic implant material, Mg can not only promote fixation but also accelerate bone repair. Based on these characteristics, Mg is also considered an alternative tissue-engineered scaffold biomaterial [19,20].

For the repair of bone defects, vascularization plays an important role in the formation of new bone [4]. Blood vessels transport nutrients to bone cells in bone tissues and carry metabolites at the same time to ensure that the new bone tissue formed is always in a healthy state [21]. Many studies have also investigated the integration of angiogenic agents with biomaterials used in bone repair to regenerate bone defects [22–24]. For example, VEGF can induce the differentiation of stem cells into vascular endothelial cells and induce the migration, differentiation and formation of microtubule structures in endothelial cells in surrounding tissues [25,26]. Its role in promoting the formation of new blood vessels is well known. VEGF can also promote the migration, proliferation and differentiation of osteoblasts; therefore, VEGF is a very important factor in the process of bone repair [27]. Based on this, the use of VEGF in the field of bone tissue engineering biomaterials has been widely studied [28,29]. There are many binding modes between growth factors and biomaterials, and different binding modes have different effects on the release kinetics of growth factors and the maintenance of bioactivity. For example, the growth factors carried by physically adsorbed deposits and hydrogels maintain their bioactivity well, but the release of high amounts of the growth factors during the initial phase after biomaterial implantation remains problematic [30]. Covalent immobilization can stabilize growth factors on site, but chemical immobilization may destroy the functional bonds of growth factors, resulting in the loss of factor bioactivity [31]. Dopamine-assisted immobilization is an emerging and promising strategy for delivering drugs [32]. Chye Khoo Poh et al. successfully immobilized VEGF on the surface of Ti by DOPA and verified that immobilized VEGF maintained its bioactivity by inducing the differentiation of stem cells into endothelial cells [33]. The rapid degradation rate of Mg has always been an important problem that needs to be solved before Mg can be used as an orthopedic implant biomaterials [19]. The degradation of Mg causes the surrounding environment to be highly alkaline, which has a negative impact on the bioactivity of VEGF [34]. Coatings are commonly used to

improve the corrosion resistance of Mg based metallic materials [35]. The chemical composition of hydroxyapatite (HA) is similar to that of bone inorganic salts, so HA coatings are widely studied as surface coating of Mg [36]. However, when HA coating is prepared on biodegradable Mg-based metallic materials, the resulting coating is usually a calcium-deficient HA (CDHA) layer (calcium and phosphorus with an atomic ratio ranging from 1.33 to 1.65). This is mainly due to the high ionization tendency of Mg, which leads to the inevitable corrosion of Mg based materials in aqueous solution, and the released Mg^{2+} ions can replace Ca^{2+} ions in HA structure. It is reported that CDHA seems to be more soluble than stoichiometric HA coating and may induce precipitation of new bone-like apatite after implantation, which just meets the requirements for biodegradable implants [37].

In this study, a protective CDHA coating was first prepared on the surface of Mg by hydrothermal treatment, and VEGF was then bound on the CDHA coating by means of DOPA covalent bonds, thus obtaining a VEGF-DOPA-CDHA coating, which was expected to endow Mg with the ability to induce angiogenesis. The changes in the surface morphology and chemical composition of the surface before and after surface modification were characterized by SEM, EDS, FTIR and XPS. ELISA and immunofluorescence experiments were conducted to confirm that VEGF bound to the surface of Mg. An immersion experiment was performed to monitor the pH change in SBF caused by Mg degradation. The biocompatibility and angiogenesis of the VEGF-DOPA-CDHA coating were verified by *in vitro* cell experiments.

2. Materials and methods

2.1. Materials

Extruded high-purity Mg (HP Mg) rods (≥ 99.99 wt%) were provided by Dongguan Eontec Co., Ltd., China. Mg discs (denoted as Mg) with a diameter of 10 mm and a thickness of 3 mm were cut from the extruded Mg rod by electric sparking. The Mg discs were ground with SiC sand paper with a grit of 400, followed by paper with grits of 800, 1200, and 2000. The Mg discs were then ultrasonically rinsed sequentially with ethanol and distilled water for 5 min each and dried in warm air. Dopamine hydrochloride, ethylenediaminetetraacetic acid calcium disodium salt hydrate (Ca-EDTA), potassium phosphate monobasic (KH_2PO_4) and sodium hydroxide (NaOH) were purchased from Sigma–Aldrich Chemical Co. Recombinant rat VEGF was purchased from PeproTech, Inc. The live/dead cell viability kit was purchased from Life Technologies™ (California, US). The rhodamine-phalloidin kit was purchased from Cytoskeleton Inc. (Denver, USA). The recombinant rat VEGF ELISA kit was purchased from R&D Systems (Minneapolis, US). The BD Matrigel™ Basement Membrane Matrix was purchased from BD Biosciences (New Jersey, US). The FITC-conjugated polyclonal goat anti-mouse IgG antibody was purchased from Abcam (Cambridge, UK). The unconjugated monoclonal mouse antihuman von Willebrand Factor (vWF) antibody and PECAM1 (CD31) were purchased from Abcam (Cambridge, UK).

2.2. Sample preparation

First, hydrothermal treatment was carried out to fabricate a CDHA coating on the surface of Mg as previously reported (hereafter referred to as CDHA-Mg). In brief, a solution containing 0.25 M Ca-EDTA and KH_2PO_4 was placed in an autoclave, and the pH of the solution was adjusted to 8.9 using a 5 M NaOH solution. The hydrothermal treatment was carried out at 90 °C for 6 h. Subsequently, polydopamine was anchored to the CDHA coating via immersion of the hydrothermally treated specimens in a 2 mg/ml solution of dopamine (10 mM Tris buffer, pH = 8.5) overnight in the dark (hereafter referred to as DOPA-CDHA-Mg). Finally, the specimens were bound with VEGF by immersion in PBS containing 160 ng/ml VEGF for 3 h at 4 °C (hereafter referred to as VEGF-DOPA-CDHA-Mg).

2.3. Physicochemical characterizations of the coatings

SEM and EDS were used to characterize the surface morphologies and chemical compositions of CDHA-Mg, DOPA-CDHA-Mg and VEGF-DOPA-CDHA-Mg. The surface chemical structures of CDHA-Mg, DOPA-CDHA-Mg and VEGF-DOPA-CDHA-Mg were determined with Fourier transform infrared spectroscopy (FTIR, Hyperion 3000). The FTIR spectrum was recorded between 4000 and 500 cm^{-1} . The surface elemental composition was studied using X-ray photoelectron spectroscopy (XPS, Epyrean-100). To assess rhVEGF, coatings were incubated with a FITC-conjugated rabbit anti-mouse IgG antibody (diluted 1:200, Alexa Fluor 488, NOVUS Biologicals) overnight at room temperature. Immunofluorescent VEGF was viewed with a fluorescence microscope (CLSM510, Zeiss, USA). To determine the binding efficiency of VEGF on the DOPA membrane, the concentration of VEGF in the solution before and after VEGF binding on the sample surface was measured by an enzyme-linked immunosorbent method using an ELISA kit according to the manufacturer's instructions. By determining the initial and remaining amounts of VEGF loaded in PBS before and after immersion, the amount of VEGF bound on the surface of the sample was calculated.

In this study, SBF was used as the solution for the immersion experiment. SBF was prepared according to Kokubo's protocol [38]. The ratio of the volume of the soaking solution to the sample surface area was 1.25 ml/cm^2 . CDHA-Mg, DOPA-CDHA-Mg and VEGF-DOPA-CDHA-Mg were placed in SBF at 37 °C, and the immersion solution was changed every two days. On days 1, 4, 7, 10, 15, 18 and 21, pH changes of the immersion solution were recorded. The amount of VEGF in the VEGF-DOPA-CDHA-Mg immersion solution was also measured by the ELISA method. PBS was used as immersion solution to characterize the release kinetics of Mg^{2+} . The ratio of the volume of the PBS to the sample surface area was 1.25 ml/cm^2 . On days 1, 4, 6, 8, 10, 12 and 14, the concentration of Mg^{2+} in the immersion solution were recorded.

2.4. In vitro biocompatibility and bioactivity

2.4.1. Cell culture

The MC3T3-E1 cell line (murine calvarial osteoprogenitor cell line) and rat bone mesenchymal stem cells (rBMSCs) were cultured in MEM/EBSS supplemented with 10 % fetal bovine serum (FBS, Gibco), 100 U/mL penicillin and 100 $\mu\text{g}/\text{ml}$ streptomycin.

2.5. Cell viability and proliferation assay

A pool of MC3T3-E1 cells was thawed from a liquid nitrogen cell bank, expanded in a cell culture flask, and harvested upon reaching confluence. After three passages, 500 μL of a cell suspension containing 5×10^4 cells was drop-seeded onto the surfaces of CDHA-Mg, DOPA-CDHA-Mg, and VEGF-DOPA-CDHA-Mg samples in 48-well culture plates. Then, the culture plates were placed in an incubator at 37 °C and 5 % CO_2 , and the medium was changed every two days.

The proliferation of MC3T3-E1 cells on the surfaces of CDHA-Mg, DOPA-CDHA-Mg, and VEGF-DOPA-CDHA-Mg was characterized by CCK-8. At 1, 4, and 7 days, the culture medium was removed, fresh medium containing a 10 % volume of CCK-8 reagent was added to each well, and the cells were incubated for 4 h. One hundred microliters of culture medium was transferred into a 96-well plate, and the optical density was measured with a microplate reader at 450 nm.

The biocompatibilities of CDHA-Mg, DOPA-CDHA-Mg and VEGF-DOPA-CDHA-Mg samples were observed by live/dead staining (LIVE/DEAD cell viability kit, Life Technologies). MC3T3-E1 cells were cultured on the sample surfaces for 7 days, the culture medium was removed, and calcein AM and ethidium homodimer solutions diluted in PBS at 1:2000 and 1:1000, respectively, were added to the wells and incubated for 30 min at room temperature in the dark. The cell viabilities on the surfaces of CDHA-Mg, DOPA-CDHA-Mg and VEGF-DOPA-CDHA-Mg were determined under a fluorescence microscope.

2.6. Direct cell adhesion and spreading assay

After incubation for 24 h, rhodamine-phalloidin staining was used to observe the spreading of the MC3T3-E1 cells cultured on CDHA-Mg, DOPA-CDHA-Mg and VEGF-DOPA-CDHA-Mg. First, the specimens were fixed with 4 % paraformaldehyde in PBS for 10 min and then permeabilized with 0.2 % Triton-X 100 in PBS for 30 min. Subsequently, the specimens were washed with PBS three times. Finally, the specimens were stained with rhodamine-phalloidin for 45 min at room temperature, and nuclei were counterstained with 4',6-diamidino-2-phenylindole (DAPI) for 30 min at room temperature.

After incubation for 7 days, the samples were washed with PBS and fixed in 2.5 % v/v glutaraldehyde for 12 h at 4 °C. Then, the samples were dehydrated in alcohol at gradually increasing concentrations (50 %, 60 %, 70 %, 80 %, 90 %, 95 % and 100 % ethanol in sequence) for 10 min each, critical-point dried, and sputtered with Pt. SEM was used to observe the cell attachment morphology on the surfaces of CDHA-Mg, DOPA-CDHA-Mg and VEGF-DOPA-CDHA-Mg.

2.7. In vitro angiogenesis assay

The effect of surface modifications on the angiogenic differentiation of rBMSCs was characterized by immunostaining, real-time quantitative reverse transcriptase polymerase chain reaction (qRT-PCR) and tube formation assays.

A 500 μL cell suspension containing 2×10^5 rBMSCs was drop-seeded onto the surfaces of the CDHA-Mg, DOPA-CDHA-Mg, and VEGF-DOPA-CDHA-Mg samples in an incubator at 37 °C and 5 % CO_2 , and the culture medium was changed every two days. For immunofluorescence microscopy, rBMSCs grown on the surfaces of CDHA-Mg, DOPA-CDHA-Mg, and VEGF-DOPA-CDHA-Mg for 2 weeks were detached with trypsin. After the cells were centrifuged, 200 μL of culture medium was added, blended evenly, and dropped onto the slide overnight. After the culture medium was removed, the cells on the slide were rinsed with PBS, fixed with 4 % paraformaldehyde for 5 min, washed with PBS, permeated with 0.2 % Triton for 30 min, washed with PBS, and sealed with 10 % donkey serum for 1 h. For CD31 staining, the cells were incubated with primary anti-CD31 antibodies (1:200, Abcam) overnight at 4 °C, rinsed in PBS and further stained with FITC-conjugated goat anti-mouse secondary antibodies (1:200, Abcam). After washing with PBS, the cell nuclei were stained with DAPI. For vWF staining, the cells were incubated with a FITC-conjugated anti-vWF antibody (1:200, Abcam) overnight at 4 °C, rinsed in PBS and further stained with DAPI. The cells were then viewed by confocal microscopy.

The mRNA expression of CD31 and vWF was investigated by qRT-PCR. The rBMSCs were seeded on CDHA-Mg, DOPA-CDHA-Mg and VEGF-DOPA-CDHA-Mg at a density of 2×10^5 /well in 48-well culture plates. After culturing for 7 and 14 days, the expression of CD31 and vWF was determined to evaluate the differentiation of the cultured cells. Total RNA was extracted from the cultured cells on the samples using TRIzol reagent (Invitrogen Life Technologies) at each time point and subsequently converted into cDNA using PrimeScript RT Master Mix (Takara). RT-PCRs were performed using SYBRPremix Ex Taq II (Takara) on a CFX96 PCR system (Bio-Rad). GAPDH was used as a housekeeping gene. The primers are shown in Table 1. Expression levels were calculated based on the 2- ΔCt method by normalizing the values to that of the housekeeping gene GAPDH.

BMSCs were cultured on the surfaces of CDHA-Mg, DOPA-CDHA-Mg

Table 1
Primers Used in qRT-PCR.

Gene	Forward primer sequence (5'-3')	Reverse primer sequence (5'-3')
GAPDH	GAAGGCAGCCCTGGTAACC	ATGGTGGTGAAGACGCCAGTAA
CD31	CAGCGTTCAACAGAGCCAGCAT	CTTCCACGGAGCAAGAAAGACT
vWF	GTCGGAAGAGGAAGTGGACATT	GGGCACACGCATGCGCTCTGTA

and VEGF-DOPA-CDHA-Mg for 14 days. The cells were detached by trypsin and centrifuged. Two hundred microliters of culture medium was added to obtain the cell suspension. After counting, culture medium was added to dilute the cell suspension to 4×10^4 cells/mL, and 50 μ L of BD Matrigel was added to a 96-well plate. After being placed in a 37 °C incubator for 1 h, the BD Matrigel solidified. Fifty microliters of the cell suspension (containing 2000 cells) was added to the surface of the Matrigel and incubated for 3 h. For the tube formation assay, the cells were stained by live/dead staining (LIVE/DEAD cell viability kit, Life Technologies), then the formation of microtubules was observed under a fluorescence microscope. For alpha-smag staining, the cells on the matrigel were rinsed with PBS, fixed with 4 % paraformaldehyde for 5 min, washed with PBS, permeated with 0.2 % Triton for 30 min, washed with PBS, and sealed with 10 % donkey serum for 1 h. For alpha-smag staining, the cells were incubated with primary anti-alpha-smag antibodies (1:200, Abcam) overnight at 4 °C, rinsed in PBS and further stained with FITC-conjugated goat anti-mouse secondary antibodies (1:200, Abcam). After washing with PBS, the cell nuclei were stained with DAPI. The cells were then viewed by a fluorescence microscope.

2.8. Statistical analysis

The results are presented as the mean \pm SEM for each group. One-way ANOVA followed by Bonferroni's multiple comparison test was used to statistically compare the different groups. P values < 0.05 were considered statistically significant.

3. Results

In this study, Mg was coated with a biofunctionalized composite step by step, as illustrated in Fig. 1. All of the different groups were characterized in terms of their morphology, composition, biocompatibility and angiogenic bioactivity.

As shown in Fig. 2, a CDHA coating was first prepared on the surface of Mg discs by hydrothermal treatment. The SEM images showed that the surface of the coating was uneven, and the surface morphology of the coating exhibited nanoneedle topography. The EDS results showed that part of the Ca^{2+} in the coating was replaced with Mg^{2+} and Na^+ . The ratio of Ca, Mg and Na to P was approximately 1.66, which is close to the Ca/P ratio in hydroxyapatite (HA). This result is consistent with our previous research [39]. A nanoscale CDHA coating formed on the Mg disc surfaces by hydrothermal treatment. After the CDHA-Mg was immersed in the dopamine solution, a new coating was formed on the CDHA coat. The EDS results showed a small amount of N (2.02 atomic%) in the coating. After soaking DOPA-CDHA-Mg in VEGF solution for 3 h, the surface morphology of the coating did not change much. The EDS results

showed that the N element of the coating increased to an atomic % of 4.30.

The composition of the coating was analyzed by XPS and FTIR. As shown in Fig. 3a and Table 2, characteristic P–O and O–H peaks were observed in the Raman spectrum of CDHA-Mg. Newly formed δ ring(C–H), ν PDA(C–O), ν ring(C=C) characteristic peaks were observed at wavenumbers of 896, 1280, and 1420 cm^{-1} in the FTIR pattern after CDHA-Mg was soaked in dopamine and VEGF solution. The XPS wide-scan spectra of CDHA-Mg, DOPA-CDHA-Mg and VEGF-DOPA-CDHA-Mg are shown in Fig. 3b, and their corresponding surface elemental compositions are shown in Table 3. The surface of CDHA-Mg was mainly composed of Ca, Mg, O and P. In addition, peaks of C 1s and N 1s were also observed. Carbon was typically present in the wide-scan spectrum of CDHA-Mg due to unavoidable hydrocarbon contamination. The small amount of N may have been attributed to impurities in the HA coating. For DOPA-CDHA-Mg and VEGF-DOPA-CDHA-Mg, the peak intensities of P 2p, P 2s, Ca 2p, Ca 2s and Ca KLL in the DOPA-CDHA-Mg and VEGF-DOPA-CDHA-Mg samples were significantly decreased, while the peak intensities of C 1s and N 1s were increased. The element content analysis showed the same trend, as the contents of C and N in DOPA-CDHA-Mg were higher than that of CDHA-Mg, and the contents of C and N in VEGF-DOPA-CDHA-Mg were further increased compared with that of DOPA-CDHA-Mg.

To confirm that VEGF was immobilized on the surface of the sample, immunofluorescence and ELISAs were used to qualitatively and quantitatively assess the binding of VEGF on the sample surfaces. As shown in Fig. 4a and Fig. 4b, immunofluorescence assays confirmed that VEGF was bound to the surface of the sample. Fig. 4c showed that before soaking, the concentration of VEGF in the loading solution was 165.5 ± 12.1 ng/ml. After soaking, the concentration was decreased to 16.4 ± 4.4 ng/ml. The binding efficiency of VEGF to the sample surface reached 90.1 %, and the density of VEGF bound on the sample surface was calculated to be approximately 55.8 ng/cm².

Fig. 5a–c showed the surface morphologies of CDHA-Mg, DOPA-CDHA-Mg and VEGF-DOPA-CDHA-Mg after immersion in SBF solution at 37 °C for 14 days. As for CDHA-Mg, some cracks were observed on the surface of CDHA-Mg after immersion in SBF for 14 days. It was observed that a apatite like layer was deposited on the surface of DOPA-CDHA-Mg and VEGF-DOPA-CDHA-Mg at day 14. The concentration of released Mg^{2+} from CDHA-Mg, DOPA-CDHA-Mg and VEGF-DOPA-CDHA-Mg during immerison in PBS for 14 days was shown in Fig. 5d. It can be seen that the concentration of released Mg^{2+} basically maintained between 50 and 90 ppm. Fig. 5e showed the effects of different coatings on the degradation of Mg discs were characterized by immersion experiments in SBF. After hydrothermal treatment, Mg degradation was observed based on a very limited increase in the pH of the SBF. The pH of

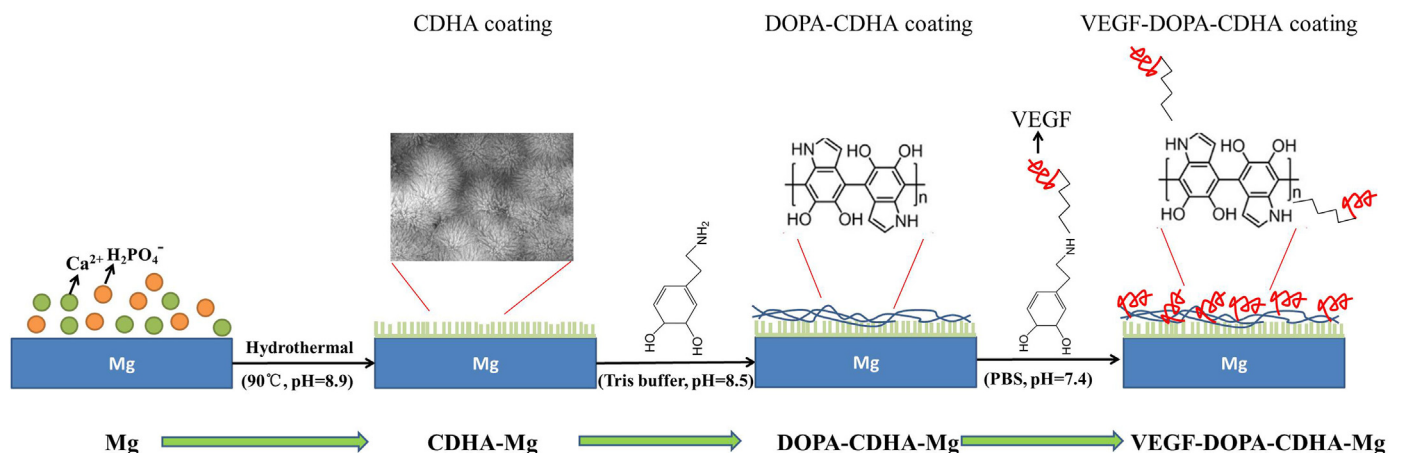


Fig. 1. Schematic illustration. Mg was coated with CDHA, DOPA-CDHA and VEGF-DOPA-CDHA via a layer-by-layer assembly method.

Table 3

Elemental composition as determined by XPS at the surface of CDHA-Mg, DOPA-CDHA-Mg and VEGF-DOPA-CDHA-Mg.

Specimens	O (at.%)	C (at.%)	P (at.%)	Ca (at.%)	Mg (at.%)	N (at.%)
CDHA-Mg	56.25	11.34	12.73	17.10	2.27	0.31
DOPA-CDHA-Mg	33.03	47.40	5.89	7.55	1.19	4.94
VEGF-DOPA-CDHA-Mg	36.12	50.03	3.01	3.83	1.00	6.01

SBF increased from 7.25 to 7.8 at the initial soaking stage and then decreased again to approximately 7.7. After dopamine film formation and VEGF immobilization, the protection of composite coatings on Mg was further improved. After soaking the samples in SBF for one day, the pH value of the simulated body fluids increased from 7.25 to approximately 7.6 and then gradually decreased, and the pH value was basically maintained at approximately 7.5 from 7 to 21 days. Moreover, the stability of the VEGF immobilized on the surface of the sample during the immersion experiment was also tested (Fig. 5). On the first day of the immersion experiment, approximately 21.4 % of the VEGF was detached from the sample surface and entered the surrounding immersion medium. Subsequently, the amount of VEGF released from the sample

surface into the soaking medium decreased rapidly, and the total amount of VEGF released from the sample surface at 21 days was approximately 31.2 %, indicating that most of the VEGF was firmly immobilized on the sample surface.

A CCK-8 assay was used to evaluate the proliferation of MC3T3-E1 cells on different coatings. As shown in Fig. 6a, there was no significant difference in the cell proliferation on different coatings on the first day. Cell proliferation was significantly greater in the VEGF-DOPA-CDHA-Mg group than in the DOPA-CDHA-Mg group at 4 days. There was no significant difference in the cell proliferation between the DOPA-CDHA-Mg and CDHA-Mg groups. On day 7, there were significant differences among all groups in the following order: VEGF-DOPA-CDHA-Mg > DOPA-CDHA-Mg > HA-Mg. Fig. 6b–d shows the fluorescence images of the attached cells on different coatings subjected to live/dead staining. The cells on different coatings were stained green, but no red color was observed, indicating that the cells on the sample surface were alive. These results verified the good biocompatibilities of the CDHA coating, DOPA-CDHA coating and VEGF-DOPA-CDHA coating.

As shown in Fig. 7a–c, the spreading area of the cells in the VEGF-DOPA-CDHA-Mg group was significantly larger than that of the other two groups. Fig. 7d–f showed the adhesion morphologies of MC3T3-E1 cells on different coatings after culture for 7 days. The cells are fully spread out on the different coatings, and the pseudopodia MC3T3-E1 are

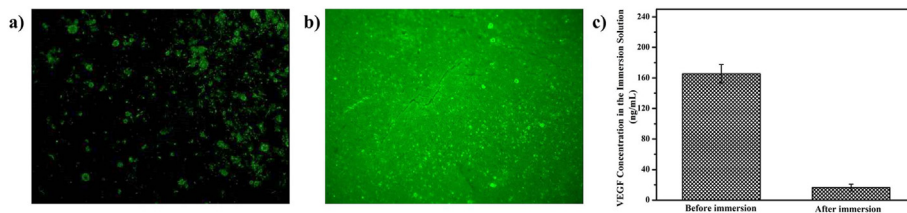


Fig. 4. (a) immunofluorescence detection of VEGF on CDHA-Mg, (b) immunofluorescence detection of VEGF on VEGF-DOPA-CDHA-Mg, (c) the amount of VEGF in PBS before and after 3 h immersion as determined by ELISA.

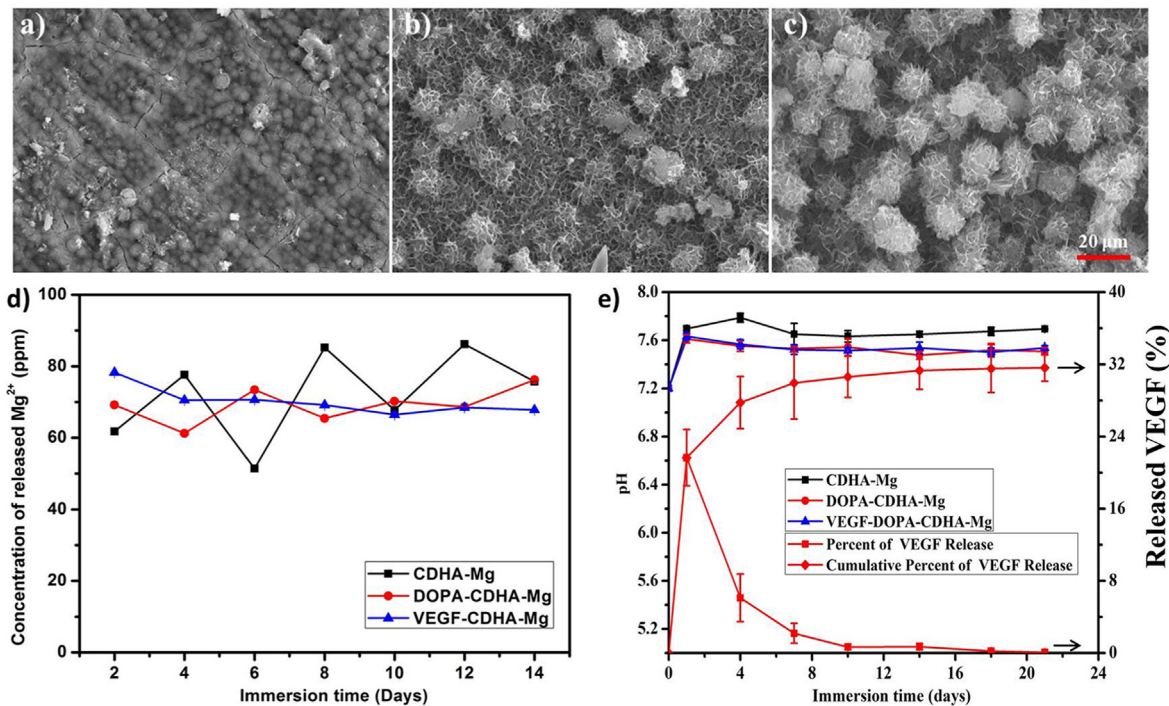


Fig. 5. Surface morphologies of CDHA-Mg (a), DOPA-CDHA-Mg (b) and VEGF-DOPA-CDHA-Mg (c) after immersion in SBF for 14 days; (d) The concentration of released Mg^{2+} from CDHA-Mg, DOPA-CDHA-Mg and VEGF-DOPA-CDHA-Mg during immersion in PBS for 14 days; (e) pH variations of CDHA-Mg, DOPA-CDHA-Mg and VEGF-DOPA-CDHA-Mg immersed in the SBF; in vitro kinetics of the VEGF release from VEGF-DOPA-CDHA-Mg.

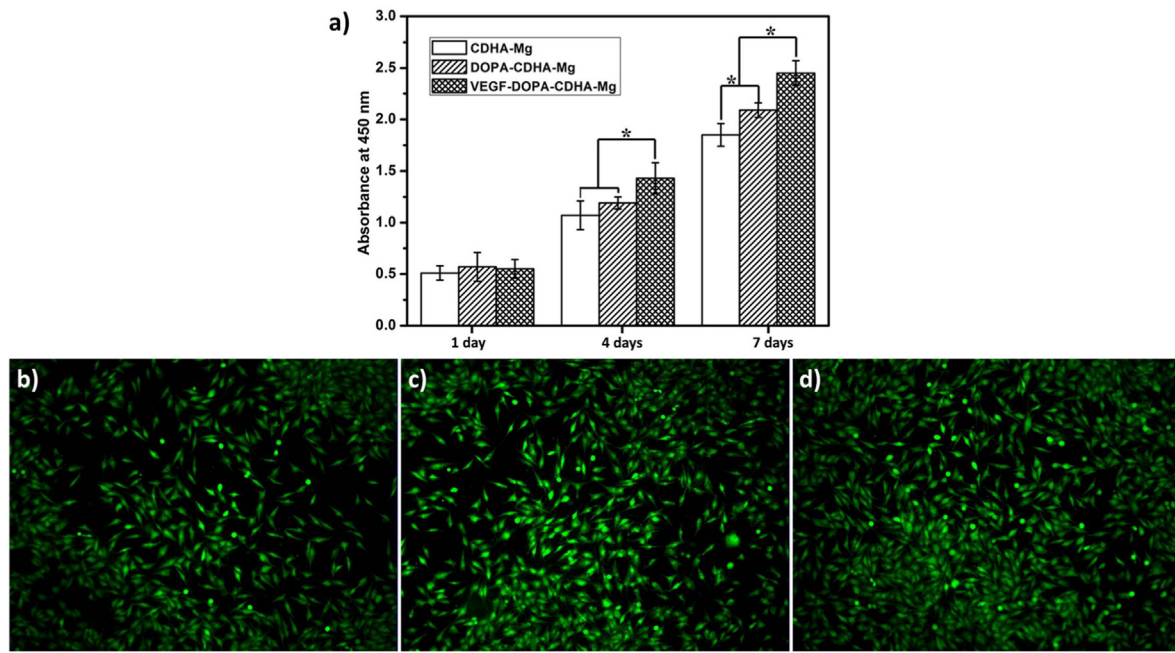


Fig. 6. a) Measurement of MC3T3-E1 cell proliferation by the CCK-8 assay after 1, 4, and 7 days of incubation on the surfaces of CDHA-Mg, DOPA-CDHA-Mg and VEGF-DOPA-CDHA-Mg. For each group, n = 3; asterisks (*) indicate statistical significance, p < 0.05; live/dead staining of MC3T3-E1 cells cultured on the surfaces of CDHA-Mg (b), DOPA-CDHA-Mg (c) and VEGF-DOPA-CDHA-Mg (d) at day 7.

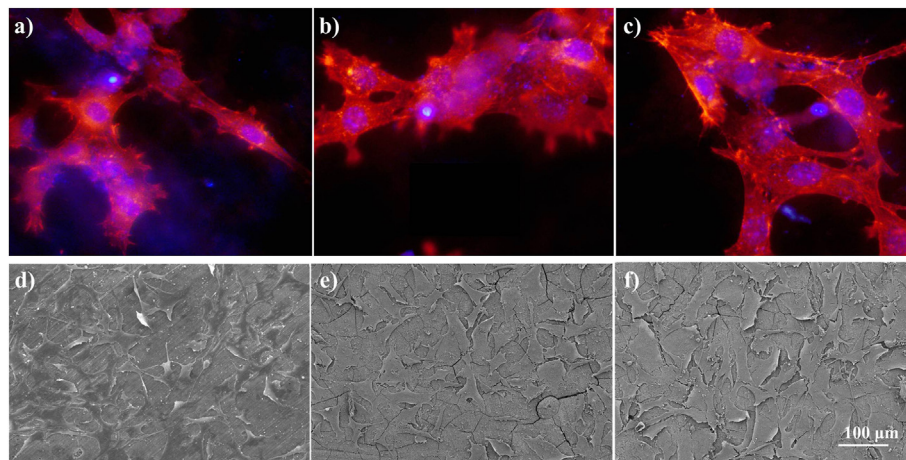


Fig. 7. Fluorescence images of actin (red) and nuclear (blue) staining of MC3T3-E1 cells cultured on CDHA-Mg (a), DOPA-CDHA-Mg (b) and VEGF-DOPA-CDHA-Mg (c) after 24 h; SEM micrographs of MC3T3-E1 cells cultured on CDHA-Mg (d), DOPA-CDHA-Mg (e) and VEGF-DOPA-CDHA-Mg (f) after 7 days.

obviously elongated.

To verify the ability of immobilized VEGF to bioactively promote vascularization, immunofluorescence was used to characterize the expression of CD31 and vWF antibodies in rBMSCs after culture for 14 days on CDHA-Mg, DOPA-CDHA-Mg and VEGF-DOPA-CDHA-Mg. As shown in Fig. 8, CD31 and vWF were significantly expressed in the rBMSCs in the VEGF-DOPA-CDHA-Mg group, while CD31 and vWF expression was basically not observable in the cells of the CDHA-Mg and DOPA-CDHA-Mg groups.

The bioactivity of immobilized VEGF on early blood vessel development was assessed by an in vitro angiogenesis assay. Fig. 9a–c shows the microtubule formation of rBMSCs in different groups. Microtubule formation was not observed for the cells on CDHA-Mg and DOPA-CDHA-Mg, while the cells on the VEGF-DOPA-CDHA-Mg sample formed obvious microtubule structures. Alpha-smag expression was also observable in the cells of the VEGF-DOPA-CDHA-Mg groups. To further investigate

angiogenic differentiation at a molecular level, the mRNA expressions of angiogenesis related genes, including vWF and CD31, were characterized by qRT-PCR analysis after co-culturing for 7 and 14 days. As shown in Fig. 9d and e, the rBMSCs on the VEGF-DOPA-CDHA-Mg had significantly higher vWF and CD31 gene expression on day 7 and day 14.

4. Discussion

Tissue engineering is a promising method for repairing bone defects larger than critical size [40]. Biochemical modifications was commonly used to functionalize biomaterials by immobilization or delivery of bioactive molecules for the purpose of inducing specific cell and tissue responses [41]. Li et al. [42] immobilized Foxy5 peptide on hydrogels to enhanced bone regeneration by activating noncanonical Wnt signaling via the up-regulation of Disheveled 2 and downstream RhoA-ROCK signaling. Zhu et al. [43] immobilized N-cadherin mimetic peptide on

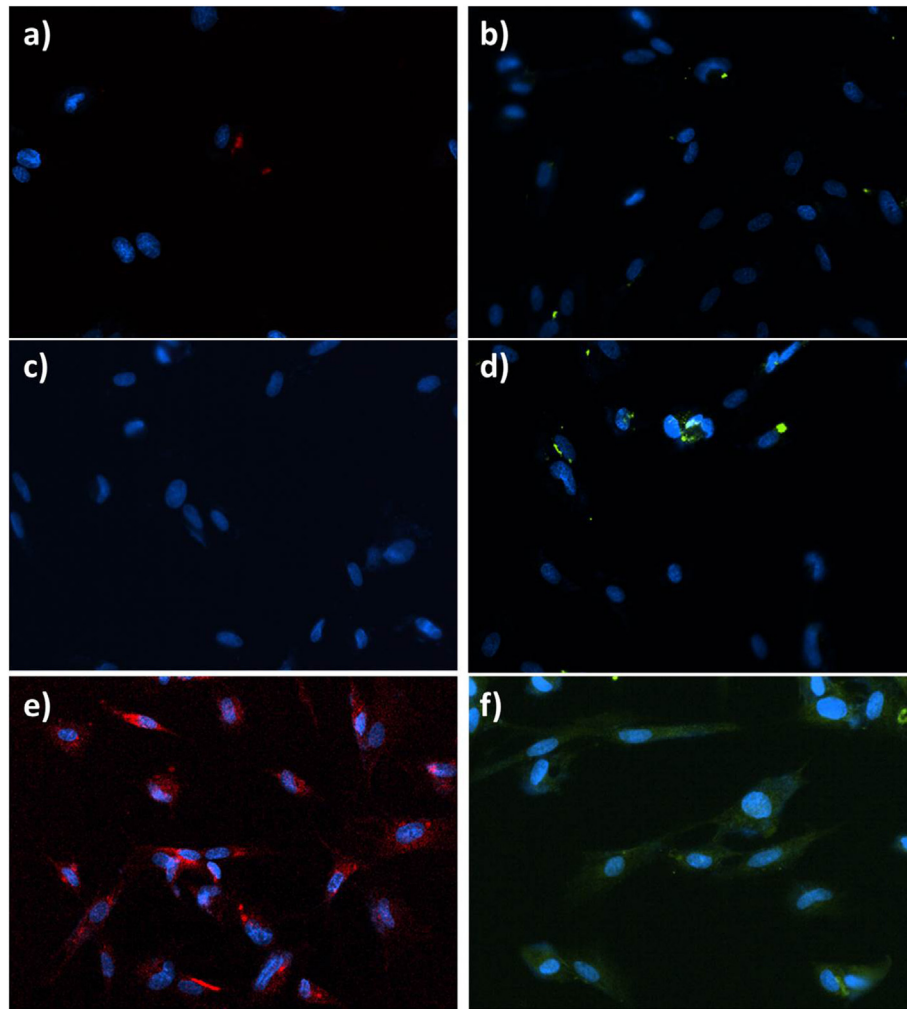


Fig. 8. Immunofluorescence staining of CD31 expression (a, c, e) and vWF expression (b, d, f) in rBMSCs cultured on CDHA-Mg (a, b); DOPA-CDHA-Mg (c, d) and VEGF-DOPA-CDHA-Mg (e, f) after 2 weeks.

Ti via the acryloyl bisphosphonate (Ac-BP) to improve the osseointegration of implants. Vascularization plays an important role in bone repair and regeneration. Hypovascularization is a major challenge for using tissue engineering methods to repair and regenerate bone defects [29]. VEGF is often used to promote the formation of blood vessels at defect sites during bone repair, and it is very important for VEGF to be continually active during bone repair [26]. In this study, Mg was selected as the matrix material for the bone repair tissue engineering scaffold. We first coated a Mg matrix with CDHA and then immobilized VEGF on the surface of CDHA-Mg using dopamine. The HA coating significantly reduced the initial degradation rate of Mg, thus prohibiting a locally high pH and allowing VEGF to remain biologically active to promote angiogenesis within a certain period of time.

There are many reports on the methods for coating Mg with HA [35, 36,44,45]. In this study, a uniform coating of CDHA with high adhesion was prepared on the surface of magnesium metal by water heat treatment, and the coating showed a nanoscale topography. The process by which CDHA is coated on Mg by the hydrothermal reaction method is simple to perform, cost a low amount and does not require expensive equipment. Moreover, the hydrothermal reaction process is carried out in a liquid environment, which is very suitable for preparing HA coatings on materials with complex shapes. In this study, a Ca-deficient HA coating was obtained, and the CDHA coating was reported to be more conducive to stem cell differentiation into osteoblasts than the HA coating [46]. Immersion experiments showed that the CDHA coating inhibited the rapid degradation of Mg within the initial three weeks, which is very

important for the repair of bone defects. On the one hand, the existence of the CDHA coating avoids the risk of osteolysis caused by excessively high local alkalinity and ensures that stem cells or osteoblasts can adhere, proliferate and differentiate on the surface of Mg in the early stage of implantation. The concentration of Mg^{2+} released from CDHA-Mg, DOPA-CDHA-Mg and VEGF-DOPA-CDHA-Mg during soaking is between 50 and 90 ppm, which is an effective concentration range for Mg^{2+} to play a role in promoting osteogenesis according to the report of Lin et al. [47] and Zhang et al. [48].

VEGF is immobilized on the CDHA coating by dopamine, which is a very stable connection mode. The immersion test results showed that approximately 21.4 % of the VEGF was released from VEGF-DOPA-CDHA-Mg on the first day of immersion. Some of the released VEGF derived from the failure of dopamine to chemically immobilize on DOPA-CDHA-Mg, and some was derived from the degradation of the CDHA coating, resulting in the release of VEGF immobilized on the coating. From the second day, the amount of VEGF released into the immersion solution significantly decreased. Within three weeks, the amount of VEGF released into the immersion solution accounted for approximately 31.2 % of the amount of VEGF immobilized on VEGF-DOPA-CDHA-Mg, indicating that most of the VEGF was still bound to the surface of VEGF-DOPA-CDHA-Mg, which ensured the continued angiogenic biological activity of VEGF-DOPA-CDHA-Mg. E. Wernike et al. incorporated VEGF into calcium phosphate ceramics by chemical adsorption and codeposition. Within 4 days, the amount of chemically adsorbed VEGF released on the material surface exceeded 80 %, and the cumulative

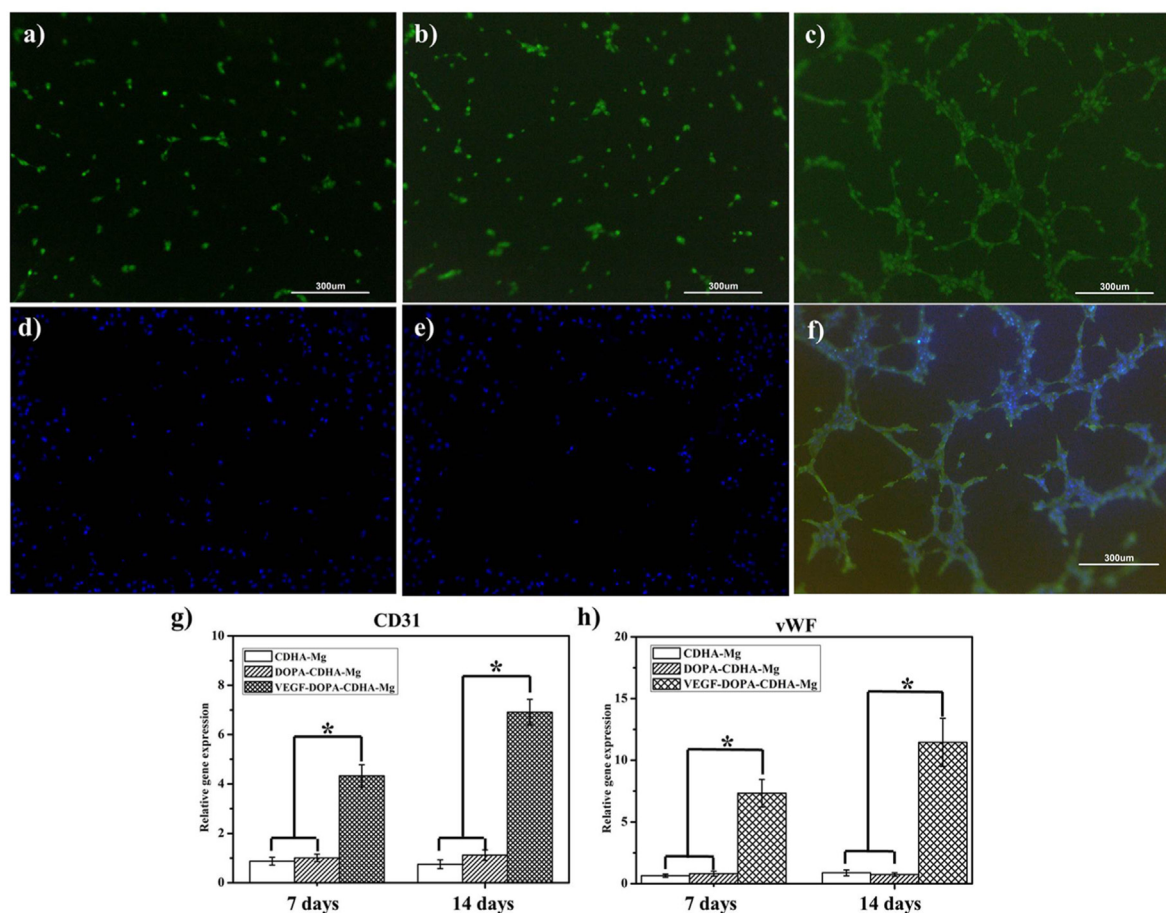


Fig. 9. In vitro microtubule formation of rBMSCs cultured on CDHA-Mg (a), DOPA-CDHA-Mg (b) and VEGF-DOPA-CDHA-Mg (c) after 2 weeks; Immunofluorescence staining of alpha-smag expression (d, e, f) in rBMSCs cultured on CDHA-Mg, DOPA-CDHA-Mg and VEGF-DOPA-CDHA-Mg after 2 weeks; qRT-PCR analyses of the CD31 (g) and vWF (h) expression levels in rBMSCs cultured on CDHA-Mg, DOPA-CDHA-Mg and VEGF-DOPA-CDHA-Mg for 7 and 14 days, $n = 3$; asterisks (*) indicate statistical significance, $p < 0.05$.

release of VEGF in the codeposition incorporated into the calcium phosphate ceramic surface was $49.6 \pm 3.7\%$ within 19 days [30]. In this study, the amount of VEGF released from VEGF-DOPA-CDHA-Mg at 21 days accounted for approximately 31.2% of the immobilized amount on VEGF-DOPA-CDHA-Mg, and 68.8% of the VEGF was still bound to its surface. The surrounding environment substantially influences the biological activity of VEGF. The rapid degradation of Mg causes the surrounding environment to be excessively alkaline, which may lead to the inactivation of VEGF [34]. In this study, Mg was first coated with CDHA by hydrothermal treatment to reduce the initial degradation rate of Mg and to ensure that the immobilized VEGF maintained its biological activity at the initial implantation stage. We studied the change in the pH of the immersion solution caused by Mg degradation through immersion experiments. The CDHA coating basically maintained the pH of the immersion solution below 7.8. The immobilization of DOPA and VEGF further increased the corrosion resistance of Mg and maintained the pH of SBF below 7.5, which is a mild environment for VEGF and is conducive to the maintenance of its bioactivity.

To verify that immobilized VEGF still has good biocompatibility, we studied the adhesion, proliferation and differentiation behaviors of rBMSCs on CDHA-Mg, DOPA-CDHA-Mg and VEGF-DOPA-CDHA-Mg in vitro. The live/dead staining results showed no dead cells on the surfaces of CDHA-Mg, DOPA-CDHA-Mg and VEGF-DOPA-CDHA-Mg, and all three coatings exhibited excellent biocompatibility. The CCK-8 and adhesion experimental results showed that DOPA and VEGF immobilization further improved the adhesion and proliferation of MC3T3-E1 cells on DOPA-CDHA-Mg and VEGF-DOPA-CDHA-Mg. Liu et al. prepared a PDA

coating on the surface of a Mg–Zn–Y–Nd alloy, which significantly improved the adhesion and proliferation of vascular smooth muscle endothelial cells on the surface of the Mg alloy [49]. The improvements in cell adhesion and proliferation on the HF-PDA-treated Mg alloy surface was attributed to the surface chemistry of the DOPA coating. The DOPA coating has abundant functional moieties, which have a good affinity for many adhesion-related proteins and nutrients in the culture medium [50]. This property promotes the adhesion and proliferation of the cells on the DOPA coating. In this study, the DOPA coating provided binding sites for the adhesion of MC3T3-E1 cells by adsorbing cell adhesion-related proteins (such as vitronectin and fibronectin) to improve cell adhesion. At the same time, the DOPA coating was conducive to the enrichment of nutrients in the medium on the coating surface, which promoted cell proliferation. The CCK-8 results showed that the proliferation of MC3T3-E1 cells on VEGF-DOPA-CDHA-Mg was superior to that on DOPA-CDHA-Mg. The effect of VEGF on promoting the proliferation of primary human osteoblasts has been reported. U. Mayr-Wuhlfart et al. found that VEGF can promote the proliferation of primary human osteoblasts within the range of 0.1–100 ng/ml in vitro [51]. VEGF regulates cell proliferation via the VEGFR-2 receptor on the cell membrane. The signal-transducing receptor VEGFR-2 is expressed on the cell membrane of osteoblasts and primary osteoblastic cells.

The purpose of this study was to immobilize VEGF on Mg to enable its biological ability to induce angiogenesis. The conformational change in VEGF immobilization on Mg and the local alkaline environment generated by Mg degradation may affect the biological activity of VEGF in angiogenesis. Chye Khoo Poh et al. immobilized VEGF on Ti via

dopamine and verified that DOPA-immobilized VEGF still had angiogenic bioactivity [33]. The DOPA-CDHA coating had a significant protective effect on Mg, and the pH value of the immersion solution was controlled within 21 days at approximately 7.5, which is a relatively mild environment for VEGF. After 14 days of rBMSC culture on CDHA-Mg, DOPA-CDHA-Mg and VEGF-DOPA-CDHA-Mg, rBMSCs grown on CDHA-Mg, DOPA-CDHA-Mg and VEGF-DOPA-CDHA-Mg for 2 weeks were seeded onto a Matrigel surface. The rBMSCs from VEGF-DOPA-CDHA-Mg formed a capillary network after 3 h of incubation on Matrigel (Fig. 9), and the rBMSCs from DOPA-CDHA-Mg and CDHA-Mg did not form any capillary network and remained isolated as single cells on the Matrigel. The endothelial cell markers vWF and CD31 were examined to confirm that the rBMSCs on VEGF-DOPA-CDHA-Mg indeed differentiated into endothelial cells. As shown in Fig. 8, the differentiated cells expressed strong vWF and CD31 after 2 weeks of culture on VEGF-DOPA-CDHA-Mg, while the differentiated cells rarely expressed vWF and CD31 after 2 weeks of culture on DOPA-CDHA-Mg and CDHA-Mg. The qRT-PCR results were consistent with the immunofluorescence results. After 7 and 14 days of coculture, the expression of angiogenesis-related genes in differentiated cells on VEGF-DOPA-CDHA-Mg was significantly higher than that in cells of the DOPA-CDHA-Mg and CDHA-Mg groups. Thus, the results further confirm that VEGF immobilized on VEGF-DOPA-CDHA-Mg retains its angiogenic bioactivity and may mediate endothelial differentiation.

5. Conclusion

The osteogenesis of Mg²⁺ is a major advantage of the use of Mg-based metallic biomaterials as tissue engineering scaffold materials. Angiogenesis deficiency is a key problem that urgently needs to be solved in regards to the use of tissue engineering methods to repair bone defects. In this study, we enabled the angiogenic biological activity of Mg by immobilizing VEGF on Mg. Mg was successfully coated with a functional VEGF-DOPA-CDHA composite coating. The CDHA coating significantly increased the corrosion resistance of Mg and prohibited the negative effect of excessively high local alkalinity on the biological activity of VEGF. As an intermediate layer, the DOPA coating protects Mg, and DOPA provides a binding site for VEGF so that VEGF can be firmly immobilized on Mg and give Mg angiogenic bioactivity during the initial period of implantation.

Declaration of competing interest

The authors declare that they have no known competing financial interests or personal relationships that could have appeared to influence the work reported in this paper.

Acknowledgment

This work was supported by the National Natural Science Foundation of China (grant no. 81702129 and 81672139) and the National Key R&D Program of China (grant no. 2016YFC1102000).

References

- Putra NE, Mirzaali MJ, Apachitei I, Zhou J, Zadpoor AA. Multi-material additive manufacturing technologies for Ti-, Mg-, and Fe-based biomaterials for bone substitution. *Acta Biomater* 2020;109:1–20.
- Ho-Shui-Ling A, Bolander J, Rustom LE, Johnson AW, Luyten FP, Picart C. Bone regeneration strategies: engineered scaffolds, bioactive molecules and stem cells current stage and future perspectives. *Biomaterials* 2018;180:143–62.
- Zhang L, Yang G, Johnson BN, Jia X. Three-dimensional (3D) printed scaffold and material selection for bone repair. *Acta Biomater* 2019;84:16–33.
- Marrella A, Lee TY, Lee DH, Karuthedom S, Syla D, Chawla A, et al. Engineering vascularized and innervated bone biomaterials for improved skeletal tissue regeneration. *Mater Today* 2017;21:362–76.
- Kelly CN, Miller AT, Hollister SJ, Guldberg RE, Gall K. Design and structure-function characterization of 3D printed synthetic porous biomaterials for tissue engineering. *Adv Healthc Mater* 2018;7(7):e1701095.
- Chen Q, Thouas GA. Metallic implant biomaterials. *Mater Sci Eng R Rep* 2015;87:1–57.
- Han Q, Wang C, Chen H, Zhao X, Wang J. Porous Tantalum and Titanium in Orthopedics: A Review. *ACS Biomater Sci Eng* 2019;5(11):5798–824.
- Wauthle R, van der Stok J, Amin Yavari S, Van Humbeeck J, Kruth JP, Zadpoor AA, et al. Additively manufactured porous tantalum implants. *Acta Biomater* 2015;14:217–25.
- Guo Y, Xie K, Jiang W, Wang L, Li G, Zhao S, et al. In vitro and in vivo study of 3D-printed porous tantalum scaffolds for repairing bone defects. *ACS Biomater Sci Eng* 2018;5(2):1123–33.
- Bandyopadhyay A, Mitra I, Shivaram A, Dasgupta N, Bose S. Direct comparison of additively manufactured porous titanium and tantalum implants towards in vivo osseointegration. *Addit Manuf* 2019;28:259–66.
- Wieding J, Lindner T, Bergschmidt P, Bader R. Biomechanical stability of novel mechanically adapted open-porous titanium scaffolds in metatarsal bone defects of sheep. *Biomaterials* 2015;46:35–47.
- Zhang B, Pei X, Zhou C, Fan Y, Jiang Q, Ronca A, et al. The biomimetic design and 3D printing of customized mechanical properties porous Ti6Al4V scaffold for load-bearing bone reconstruction. *Mater Des* 2018;152:30–9.
- Wang H, Su K, Su L, Liang P, Ji P, Wang C. Comparison of 3D-printed porous tantalum and titanium scaffolds on osteointegration and osteogenesis. *Mater Sci Eng C Mater Biol Appl* 2019;104:109908.
- Stewart C, Akhavan B, Wise SG, Bilek MMM. A review of biomimetic surface functionalization for bone-integrating orthopedic implants: mechanisms, current approaches, and future directions. *Prog Mater Sci* 2019;106.
- Zhao D, Witte F, Lu F, Wang J, Li J, Qin L. Current status on clinical applications of magnesium-based orthopaedic implants: a review from clinical translational perspective. *Biomaterials* 2017;112:287–302.
- Zhang Y, Xu J, Ruan YC, Yu MK, O'Laughlin M, Wise H, et al. Implant-derived magnesium induces local neuronal production of CGRP to improve bone-fracture healing in rats. *Nat Med* 2016;22(10):1160–9.
- Zhao D, Huang S, Lu F, Wang B, Yang L, Qin L, et al. Vascularized bone grafting fixed by biodegradable magnesium screw for treating osteonecrosis of the femoral head. *Biomaterials* 2016;81:84–92.
- Li J, Qin L, Yang K, Ma Z, Wang Y, Cheng L, et al. Materials evolution of bone plates for internal fixation of bone fractures: a review. *J Mater Sci Technol* 2020;36:190–208.
- Yang Y, He C, Dianyu E, Yang W, Qi F, Xie D, et al. Mg bone implant: features, developments and perspectives. *Mater Des* 2020:185.
- Yazdimamaghani M, Razavi M, Vashaei D, Moharamzadeh K, Boccaccini AR, Tayebi L. Porous magnesium-based scaffolds for tissue engineering. *Mater Sci Eng C Mater Biol Appl* 2017;71:1253–66.
- Fan H, Zeng X, Wang X, Zhu R, Pei G. Efficacy of prevascularization for segmental bone defect repair using β -tricalcium phosphate scaffold in rhesus monkey. *Biomaterials* 2014;35(26):7407–15.
- Wang B, Huang Y, Huang Z, Wang H, Chen J, Pan X, et al. Self-assembling in situ gel based on lyotropic liquid crystals containing VEGF for tissue regeneration. *Acta Biomater* 2019;99:84–99.
- Izquierdo-Barba I, Santos-Ruiz L, Becerra J, Feito MJ, Fernandez-Villa D, Serrano MC, et al. Synergistic effect of Si-hydroxyapatite coating and VEGF adsorption on Ti6Al4V-ELI scaffolds for bone regeneration in an osteoporotic bone environment. *Acta Biomater* 2019;83:456–66.
- Wu Y, Fu R, Mohanty S, Nasser M, Guo B, Ghosh G. Investigation of integrated effects of hydroxyapatite and VEGF on capillary morphogenesis of endothelial cells. *ACS Appl Bio Mater* 2019;2:2339–46.
- Santos MI, Reis RL. Vascularization in bone tissue engineering: physiology, current strategies, major hurdles and future challenges. *Macromol Biosci* 2010;10(1):12–27.
- Hu K, Olsen BR. The roles of vascular endothelial growth factor in bone repair and regeneration. *Bone* 2016;91:30–8.
- Sharon JL, Puleo DA. Immobilization of glycoproteins, such as VEGF, on biodegradable substrates. *Acta Biomater* 2008;4(4):1016–23.
- Wu L, Gu Y, Liu L, Tang J, Mao J, Xi K, et al. Hierarchical micro/nanofibrous membranes of sustained releasing VEGF for periosteal regeneration. *Biomaterials* 2020;227:119555.
- Zeng Y, Hoque J, Varghese S. Biomaterial-assisted local and systemic delivery of bioactive agents for bone repair. *Acta Biomater* 2019;93:152–68.
- Wernike E, Montjovent M, Liu Y, Wismeijer D, Hunziker E, Siebenrock K, et al. VEGF incorporated into calcium phosphate ceramics promotes vascularisation and bone formation in vivo. *Eur Cell Mater* 2010;19(3).
- Hu X, Neoh KG, Zhang J, Kang ET, Wang W. Immobilization strategy for optimizing VEGF's concurrent bioactivity towards endothelial cells and osteoblasts on implant surfaces. *Biomaterials* 2012;33(32):8082–93.
- Qiu WZ, Yang HC, Xu ZK. Dopamine-assisted co-deposition: an emerging and promising strategy for surface modification. *Adv Colloid Interface Sci* 2018;256:111–25.
- Poh CK, Shi Z, Lim TY, Neoh KG, Wang W. The effect of VEGF functionalization of titanium on endothelial cells in vitro. *Biomaterials* 2010;31(7):1578–85.
- Ferrara N, Gerber H-P, LeCouter J. The biology of VEGF and its receptors. *Nat Med* 2003;9(6):669–76.
- Shadanbaz S, Dias GJ. Calcium phosphate coatings on magnesium alloys for biomedical applications: a review. *Acta Biomater* 2012;8(1):20–30.
- Dorozhkin SV. Calcium orthophosphate coatings on magnesium and its biodegradable alloys. *Acta Biomater* 2014;10(7):2919–34.

- [37] Wang H, Zhu S, Wang L, Feng Y, Ma X, Guan S. Formation mechanism of Ca-deficient hydroxyapatite coating on Mg–Zn–Ca alloy for orthopaedic implant. *Appl Surf Sci* 2014;307:92–100.
- [38] Kokubo T, Takadama H. How useful is SBF in predicting in vivo bone bioactivity? *Biomaterials* 2006;27(15):2907–15.
- [39] Li J, Xu W, Lin X, Cao F, Yang J, Li L, et al. A Ca-deficient Ca-deficient hydroxyapatite (CDHA)/MgF₂ bi-layer coating with unique nano-scale topography on biodegradable high-purity Mg. *Colloids Surf B Biointerfaces* 2020;190:110911.
- [40] Wubneh A, Tsekoura E, Ayranci C, Uludağ H. Current state of fabrication technologies and materials for bone tissue engineering. *Acta Biomater* 2018;80:1–30.
- [41] Chen C, Zhang S-M, Lee I-S. Immobilizing bioactive molecules onto titanium implants to improve osseointegration. *Surf Coating Technol* 2013;228:S312–7.
- [42] Li R, Lin S, Zhu M, Deng Y, Chen X, Wei K, et al. Synthetic presentation of noncanonical Wnt5a motif promotes mechanosensing-dependent differentiation of stem cells and regeneration. *Science Advances* 2020;5:3896.
- [43] Zhu M, Zhang K, Feng L, Lin S, Pan Q, Bian L, et al. Surface decoration of development-inspired synthetic N-cadherin motif via Ac-BP promotes osseointegration of metal implants. *Bioact Mater* 2021;6(5):1353–64.
- [44] Shen S, Cai S, Bao X, Xu P, Li Y, Jiang S, et al. Biomimetic fluoridated hydroxyapatite coating with micron/nano-topography on magnesium alloy for orthopaedic application. *Chem Eng J* 2018;339:7–13.
- [45] Pang S, He Y, He P, Luo X, Guo Z, Li H. Fabrication of two distinct hydroxyapatite coatings and their effects on MC3T3-E1 cell behavior. *Colloids Surf B Biointerfaces* 2018;171:40–8.
- [46] Gustavsson J, Ginebra MP, Engel E, Planell J. Ion reactivity of calcium-deficient hydroxyapatite in standard cell culture media. *Acta Biomater* 2011;7(12):4242–52.
- [47] Lin Z, Wu J, Qiao W, Zhao Y, Wong KHM, Chu PK, et al. Precisely controlled delivery of magnesium ions thru sponge-like monodisperse PLGA/nano-MgO-alginate core-shell microsphere device to enable in-situ bone regeneration. *Biomaterials* 2018;174:1–16.
- [48] Zhang X. Ion channel functional protein kinase TRPM7 regulates Mg ions to promote the osteoinduction of human osteoblast via PI3K pathway: in vitro simulation of the bone-repairing effect of Mg-based alloy implant. *Acta Biomater* 2017;63.
- [49] Liu X, Zhen Z, Liu J, Xi T, Zheng Y, Guan S, et al. Multifunctional MgF₂/polydopamine coating on Mg alloy for vascular stent application. *J Mater Sci Technol* 2015;31(7):733–43.
- [50] Killian MS, Wagener V, Schmuki P, Virtanen S. Functionalization of metallic magnesium with protein layers via linker molecules. *Langmuir* 2010;26(14):12044–8.
- [51] Mayr-wohlfart U, Waltenberger J, Hausser H, Kessler S, Günther KP, Dehio C, et al. Vascular endothelial growth factor stimulates chemotactic migration of primary human osteoblasts. *Bone* 2002;30(3):472–7.